Metallurgical Waste as Valuable Component of Construction Materials Production

Vsevolod Mymrin*, Kirill Alekseev, Walderson Klitzke, Monica A. Avanci,

Daniela E. Pedroso, Cleber L. Pedroso, Karina Q. Carvalho, Rodrigo E. Catai

Department of Mechanical Engineering, Federal University of Technology, Parana, Brazil

Research Article

ABSTRACT

This paper reports the development and characterization of new ceramics from hazardous bauxite tailing Red Mud (50 wt.%-100 wt.%) and blast furnace slag (10%-50%). The research aimed to demonstrate the possibility of expanding the base of powder raw materials for production of ceramics, completely replacing the traditional clay and sand with composites made from hazardous industrial wastes, which provide increasing local and global sustainability. The investigation of the physical-chemical changes in the ceramics structure was conducted by the AAS, XRD, SEM, XRF, LAMMA, and EDS tests. Changes in water absorption, density, linear shrinkage, and flexural strength were determined while the sintering processes ranged from 1,000°C to 1,225°C. Flexural strength reached 19.78 MPa after sintering at 1,225°C due to the syntheses of new structure formations, mainly similar to glass, confirmed by the characterization methods used, attesting to the complete binding of heavy metals.

Keywords: Hazardous bauxite tailing red mud; Dumped ferrous slags; Industrial waste cycling; Sustainable ceramics production; Waste management; Environment protection

INTRODUCTION

In one of his interviews, the most celebrated modern-day cosmologist, S.W. Hawking [1] said that "pollution and human "stupidity" remained the greatest threats to humankind." He claimed that air pollution had increased 8% within the last five years, and the authors of this paper are convinced that most of that is due to the municipal and industrial wastes.

According to the authors of this article, the best strategic way to prevent or postpone as much as possible this global ecological tragedy, scientifically predicted by Hawking, is to replace the raw materials with industrial waste. Hawking calculated that, at the current pace, the temperature of the atmosphere would rise, leading to the death of humankind in the next 300 years. It is known that the most significant air pollutants come from industrial and municipal waste dumps. From this, it follows that the scientifically based waste disposal will be a crucial factor for the survival of humanity.

The residues from bauxite processing, called Red Mud (RM), are generated during the obtaining of aluminium oxide from the bauxite ore by the Bayer process. The World Aluminium database [2] mentions that approximately 15 to 20 million tons of aluminium wastes (RM) have been discharged into industrial wastes worldwide. In Hungary, an RM storage dam collapsed, flooding the streets with red mud, killing ten people [3]. There are two main reasons to classify this Red Mud as a hazardous material: the first one is the high pH of sodium oxide followed by the heavy metals content (Cd, Pb, Cu, Cr, Zn).

Other similar accidents have occurred involving these types of waste. The two most recent of them, in 2015 and 2019, were the overflow of iron ore tailings in Brazil [4]. The number of their victims is hundreds of people, and the economic damage is in the order of several billion dollars.

The storage of wastes presents the risk of further accidents, forcing us to accept the need to recycle or reuse them instead of storing them. This paper presents a practical, scientifically based solution to the problem of hazardous RM by using it in different composites with Ferrous Slag (FS) to produce environmentally clean ceramics.

Some articles have been written [5,6] describing the physical-chemical characteristics of RM to find its best use. It is possible to use RM to remove Mn and As from drinking water; or as an adsorbent for enhancing ferricyanide removal [7]; or in mixes with fly ash to reduce CO_2 emissions [8]. Dodoo-Arhin, et al. [9] suggested mixtures of natural clay and RM, and investigated their optimal proportions. Liu, et al. [10] treated RM for the extraction of metals and other elements. Rychkov, et al. [11] described a technology of scandium separation from Red Mud by carbonate treatment. The main flaw in this approach was that it led to the generation of more massive amounts of residue. Pontikes, et al. [12] used RM in cementitious materials production.

"Globally, the manufacture of 1.65 billion tonnes of iron and steel gives rise to the co-production of more than 567 million tonnes of metallurgical slag" [13]. Blast Furnace Slag (FS) from steel production already has some forms of implementation as a raw material. Lukowski, et al. [14] used it for binding materials' production. Barreto, et al. [15] formulated compositions with high contents of heavy metals with ornamental rocks solid waste. Solidification and stabilization of galvanic solid waste, concomitantly with ornamental rocks solid waste. There are many published studies on methods [16] and effectiveness [17] of heavy metals adsorption from diverse industrial wastes. Fertilizers made of steelmaking slag are important inexpensive materials for recovering degraded paddy fields [18]. FS was added to ceramic mixtures [19]. The above review of the scientific

and technical literature shows the originality of our ceramic compositions, which consist of only two types of hazardous industrial waste for the production of sustainable ceramic materials.

Three main objectives were sought in this study:

➢ To develop new composites using only Red Mud (RM) and ground cooled blast Furnace Slag (FS), replacing the traditional known raw materials such as sand and natural clay (CSM).

➢ To develop ceramics that meet Brazilian standards for physical, mechanical, and environmental properties.

➢ To study and to intensify the processes involved in the new structures formation, responsible for the achievement of these properties in ceramics.

MATERIALS AND METHODS

RM and FS were pre-dried at 105ºC for 24 hours to constant weight and sifted through a 1.2 mm sieve. The dry components were manually homogenized in the proportions presented in Tables 1-3 and moistened to a level of 12%-14%.

XRF method was conducted to find the chemical composition of the materials, XRD determined the mineralogical composition, and the morphological structure was observed by SEM analysis. In order to identify the microchemical composition of individual particles of the material, EDS analyses were performed. LAMMA method determined the isotropic composition. AAS was used to investigate possible solubilized and leached metals; the particle size distribution was determined by laser analysis. Completing the studies, flexural resistance, linear shrinkage, water absorption, and density were also performed.

The manufacture of ceramics was under the following steps: mixing the components according to the pre-established composition (Table 1); addition of water (12%-14%) to plasticize the mixes; compression of wet samples at 5 MPa, in rectangular press-forms of 60 × 20 × 10 mm size, drying to constant weight at 100ºC, sintering for 3 hours (temperatures of 800º, 900º, 1000º, 1050º,1100º,1150º, 1200º, and 1225ºC), and cooling by natural convection.

RESULTS AND DISCUSSION

Characterization

The characterization was conducted in order to determine the granulometric, mineral and chemical compositions, and morphological microstructure of the studied materials.

Chemical composition and particles size distribution: Both industrial wastes used as raw materials in the study were obtained from local factories in Brazil. The natural clay sample, mixed with 10% of sand, was obtained at a local ceramics production plant and was used in this work only as a generally accepted industry standard

Table 1. Chemical composition of the raw materials.

Oxides	Components (wt. %)			Oxides	Components (wt. %)		
	Red mud	Furnace slag	Clay-sand mix		Red mud	Furnace slag	Clay-sand mix
Fe_2O_3	29.9	62.1	6.1	Cr_2O_3	<0.1	0.3	<0.1
SiO_2	15.5	13.8	53.3	V_2O_5	0.1	0	<0.1

SO_3	0.6	10	0.1	BaO	0	0.2	0.1
Al_2O_3	21.2	2.6	24.7	P_2O_5	0	0.1	0
CaO	4.2	2.5	0.4	SnO_2	0	0.1	0
MgO	0.1	0.3	0.7	ZnO	<0.1	0.1	<0.1
Na_2O	10.3	0.9	0.1	CuO	0	0.1	0
K_2O	0.4	0.4	1	ZrO_2	0.2	<0.1	0.1
MnO	0.2	0.6	0.1	MoO_3	0	<0.1	0
TiO_2	2.4	0.4	1.4	I.L.	14.4	1.7	11.5
P_2O_5	0.6	3.5	0.1	Total	100	100	100

XRF method showed that RM consisted mainly of Fe_2O_3 (29.9 %), followed by Al_2O_3 (21.2%), SiO_2 (15.5%), and Na_2O (10.3%) (Table 1). The high ignition loss value (I.L.=14.36%) of the RM might be explained by the carbonates content, by some hydroxide OH-group and water content after undergoing Bayer's thermochemical process for bauxite ore treatment.

The metals Ni (1.26%), Sn (1.18%), Ba (0.79%), Zn (0.72%), found by the AAS method, exceeded the relevant Brazilian standards NBR 10,004[20]. RM is classified as a hazardous waste due to its high pH value (13.5) and the presence of high heavy metals content. FS contained extremely high amounts of ferrous oxides (62.1%) in addition to SiO_2 (13.8%) and SO_3 (10.0%), Al_2O_3 (2.6%), and CaO (2.5%).

Table 2. Grain size distribution in weight %, tapped density in g/cm³, and humidity (%) of the raw materials under study.

Grain size distribution			
Size (mm)	Red mud	Furnace slag	Clay-sand mix
0-0.074	0.32	1.35	89.76
0.075-0.149	1.08	17.63	5.68
0.15-0.29	13.14	66.39	3.17
0.3-0.59	46.13	14.63	1.39
0.6-1.19	39.33	0	0
≥ 1.2	0	0	0
Tapped density (g/cm³)	0.86	2.75	1.56
Humidity	32.2	3.1	9.34

The grain size classification Table 2 showed that RM had a total of particles between 0.3 and 1.2 mm equal to 85.46%. The majority of FS particles (85.37%), on the contrary, presented sizes between 0 and 0.29 mm.

Mineralogical composition: The mineralogical compositions of the raw materials, analyzed by the XRD method, were also somewhat different: RM held magnetite Fe_3O_4, hematite Fe_2O_3, and quartz SiO_2, while FS held fayalite $Fe_2 \cdot 2SiO_4$ and troilite FeS.

Both raw materials showed very weak crystal peaks and very robust X-Ray backgrounds due to the meager of crystalline structures and predominance of amorphous structures.

Thermic characteristics of the raw materials under study: The endothermic effect between 194ºC and 279ºC correlated with the endothermic effect of the Red Mud between 202ºC and 296ºC, which denoted a decrease in the loss of crystal structure water of gibbsite $Al(OH)_3$ with its transition to boehmite γ-$AlO(OH)_4$. The weight loss during this reaction of composition 7 was significantly lower (2.13%) than that of Red Mud (5.36%). The reason for this might be the content of 50% Red Mud in the original mixture and the imprecision of the selected points of the initial and final temperatures in the DTA and TGA curves [21].

The second endothermic effect of composition 7, between 279ºC and 392ºC with low tolerance, replicated another endothermic effect of the Red Mud between 296ºC and 431ºC. The concurrence of their weight loss values 1.50% and 3.10% was also quite logical and corresponded to the conversion reaction of boehmite γ-$AlO(OH)_4$ in anhydrous γ-Al_2O_3 [22]. The sharp peak of the exothermic reaction between 469ºC and 582ºC with a weight loss corresponded to 2.23% two-headed blast furnace slag exothermic effect at 413ºC-560ºC with a total weight loss of 1.47%.

The presence of 10.0% SO_3 and high iron content (62.1%) in the chemical composition of the blast furnace slag inevitably led to their combination during composition 7's heating in the forms of iron hydrates, iron sulfates, and iron sulfides.

A mild exothermic effect on red mud's DTA curve between 582ºC and 735ºC along with a 1.61% weight gain on TGA curve was probably due to the transition of anhydrous boehmite γ-Al_2O_3 to α-Al_2O_3 [21]. There was also a chain of transitions in the blast furnace slag $FeOOH \rightarrow \gamma$-$Fe_2O_3 \rightarrow Fe_3O_4$ at the same temperature [22], related to the $Fe_2(SO_4)_3$ melting and to the beginning of the combustion the SO_2 gas, which was formed due to the transition of $Fe_2(SO_4)_3$ to Fe_2O_3. The appearance of this exothermic effect in the blast furnace slag corresponded to thermochemical decomposition of FeS_2 by oxidation with the following transfer to $FeSO_4+SO_2$ and burning of the released gas. Typically, this reaction takes place at 630ºC-650ºC, which coincided with the peak's turning point at an environment of 582ºC-735ºC. The total weight increase was equal to 2.33%. The third exothermic effect of composition 7 occurred at 735ºC -1,227ºC and involved four different thermochemical reactions: The transition γ-$Al_2O_3 \rightarrow \alpha$-$Al_2O_3$; the transition $Fe_3O_4 \rightarrow Fe$ up to 700ºC-750ºC; reduction in sample weight as a result of the final SO_2 release and burning of the released gas; the formation of Fe_3O_4. The total weight loss of these processes was 4.43%.

Probably, the formation of iron dross and the SO_2 combustion process imparted the darkening of the samples, which appeared at temperatures of 1,200ºC–1,225ºC. The maximum intensity of these processes at 1,225ºC resulted in maximum flexural strength.

Morphological structures: The morphological structures of the particles suggest a wide variety of shapes, sizes, and forms of the grains of all materials, which meant that there was no uniform structure. Such particle morphology indicated a predominantly amorphous structure of the materials, established by the XRD method. All of them were disconnected and had no chemical bonds between them. A significant difference was observed between RM and FS regarding compositions (chemical and mineralogical) and particle structure.

Physical properties of new ceramics

The ceramics flexural strength changes, linear shrinkage, water absorption, and apparent density were looked into after sintering at different temperatures to characterize their physical properties.

Flexural strength of new ceramics: Red Mud was the principal component of this study. It contained the remains of the alkaline reagent from bauxite ore decomposition (hydroxide NaOH) Table 1, having a melting point (T_m) of 323ºC. This occurrence led to the formation of chemical compounds, such as $NaHCO_3$ (T_m=270ºC), Na_2CO_3.

(T_m=852ºC) and Na_2SO_4, (T_m=883ºC). Therefore, these chemical species might serve as flux components during the ceramics firing process, reducing it. Comparing the tiny increase in RM flexural strength values Table 3 at 1200ºC (12.17 MPa) and 1,225ºC (12.32 MPa), it may be stated that, at about 1,225ºC, the RM was very close to exceeding its melting point. An increase in FS content drove to a decrease in the flux of RM content and an increment in the temperature, favouring the excessive melting of ceramics.

Therefore, ceramics 7, with the highest slag content (50%), had the highest strength (19.78 MPa) after 1,225ºC firing; and ceramics 2 (without slag) and 3 (with 10% slag content) showed the lowest resistance (12.32 MPa and 13.10 MPa, respectively).

Solid bricks are classified by NBR 15270 [23] according to their flexural strength in three classes: Class A<2.5 MPa; Class B from 2.5 to 4.0 MPa; and Class C>4.0 MPa. It means that practically all developed ceramics met the demands of Class A (<2.5 MPa) after 800ºC sintering. Ceramics 3 met the requirements of Class B (2.5-4.0 MPa) after 900ºC as well as ceramics 4 and 7 after 1,000ºC and ceramics 5 after 1,050ºC. Ceramics 3, 6, and 7 after 1050ºC corresponded to the demands of Class C, as well as all other ceramics after sintering at 1,100ºC. All ceramics significantly exceeded the demands of class C (>4.0 MPa) after firing at 1,150ºC. The values of standard deviations of flexural resistance strength of samples varied between 0.5 and 1.2 MPa.

Table 3. Flexural resistance strength after sintering at different temperatures (ºC).

Compositions wt.%			Flexural strength (MPa) of ceramics after sintering at TºC							
No	CSM	RM	FS	800	900	1,000	1,050	1,100	1,150	1,200	1,225
1	100	0	0	5.36	5.68	7.09	8.72	10.08	14.65	13.36	6.05
2	0	100	0	0	0	0.45	0.93	4.34	6.06	12.17	12.32
3	0	90	10	2.21	2.66	3.13	4.24	5.51	7.42	12.27	13.1
4	0	80	20	2.27	2.44	2.64	3.62	4.65	7.81	14.28	15.96
5	0	70	30	1.26	2.08	2.34	3.15	4.72	8.49	10.65	16.36
6	0	60	40	1.21	1.67	2.26	4.3	5.01	8.1	10.11	18.05
7	0	50	50	1.59	2.17	3.34	5.39	8.12	13.05	15.55	19.78

Water absorption and apparent density: The water absorption value is an indirect indicator of the open porosity of materials, so the changes in water absorption Table 4 were also strongly linked to changes in flexural strength.

Table 4. The water absorption value of the developed ceramics.

Composites mwt.%			Water absorption (%) of ceramics at different temperatures (ºC)							
No	CSM	RM	FS	800	900	1,000	1,050	1,100	1,150	1,200	1,225
1	100	0	0	20.4	20	18.49	15.26	12.76	10.53	8.78	8.1

2	0	100	0	33.78	31.36	28.68	25.79	24.62	19.98	11.79	9.31
3	0	90	10	27.65	27.28	27.86	22.86	20.51	17.03	9.67	6.14
4	0	80	20	28.65	26.35	24.9	21.67	19.49	16.12	8.41	4.56
5	0	70	30	22.66	24.94	23.19	22.48	18.92	14.23	7.29	2.29
6	0	60	40	26.94	25.14	20.29	19.22	17.17	11.04	5.64	1.45
7	0	50	50	23.37	19.63	17.09	16.73	14.68	9.16	2.86	2.09

The water absorption values decreased with the temperature rise due to a more intense process of closure of the open pores.

Composition 7, with the maximum amount of slag, showed the lowest water absorption values at all sintering temperatures; the maximum value was found in composition 2 (100% RM). The values decreased from 33.78% to 2.09%, with standard deviations values between 0.07%-0.1%.

The changes in the apparent density of the samples Table 5 were similar to those observed for the linear shrinkage values: they grew with the increase in temperature from 1.28 g/cm^3 to 2.61 g/cm^3.

Table 5. Density of ceramic composites after firing at different temperatures (ºC).

| Compositions content wt.% | | | Density (g/cm^3) at different T (ºC) | | | | | | | |
No	CSM	RM	FS	800	900	1,000	1,050	1,100	1,150	1,200	1,225
1	100	0	0	1.56	1.58	1.61	1.7	1.77	1.84	1.87	1.8
2	0	100	0	1.28	1.31	1.35	1.42	1.44	1.55	1.89	1.96
3	0	90	10	1.38	1.42	1.47	1.5	1.56	1.62	1.82	1.87
4	0	80	20	1.47	1.52	1.55	1.58	1.65	1.72	1.99	2.16
5	0	70	30	1.53	1.59	1.64	1.62	1.72	1.81	2.26	2.47
6	0	60	40	1.71	1.75	1.77	1.77	1.82	1.97	2.24	2.54
7	0	50	50	1.85	1.88	1.9	1.9	1.96	2.14	2.4	2.51

The minimum values of density after all sintering temperatures were observed for composition 7, with the maximum amount of slag; composition 2 (100% RM) showed the maximum density value. Such behaviour was highly expected, given the ongoing shrinkage of the samples and the reduction of water absorption (porosity) as the temperature increased. Standard deviations are within the limits of 0.09 g/cm^3 and 0.4 g/cm^3.

Linear shrinkage of the developed ceramics: Changes in linear shrinkage values Table 6 were analyzed by measuring the largest linear dimensions–samples' length-after sintering at different temperatures (Figure 1). In many cases, sharp changes were strongly linked to more significant changes in flexural strength. The linear shrinkage values increased up to a temperature of maximum strength. When the melting point of a sample was exceeded, the shrinkage decreased due to the foaming of excessive melting through the changes in the color of the samples and the rounding of their edges and angles. Shrinkage values were between 0.04% and 12.54%, while their standard deviations ranged from 0.4% and 1.7%.

Table 6. Linear shrinkage of ceramics at different firing temperatures.

Composites wt.%			Linear shrinkage (%) of ceramics after sintering at different temperatures (ºC)							
No	CSM	RM	FS	800	900	1,000	1,050	1,100	1,150	1,200	1,225
1	100	0	0	5.36	5.68	7.76	9.09	10.47	11.52	11.95	11.86
2	0	100	0	1.89	2.27	3.42	4.33	5.29	7.24	11.67	12.45
3	0	90	10	0.96	1.08	1.92	2.98	4.3	5.64	9.43	9.56
4	0	80	20	0.54	0.63	0.81	1.51	2.64	4.41	7.4	11.07
5	0	70	30	0.07	0.24	0.31	0.83	2.46	4.38	11.37	12.54
6	0	60	40	0.04	0.11	0.18	0.39	1.69	5.26	12.32	12.35
7	0	50	50	0.08	0.12	0.17	0.44	1.13	4.28	10.99	11.4

Figure 1. Photo of ceramics 7 after sintering at 1,225ºC.
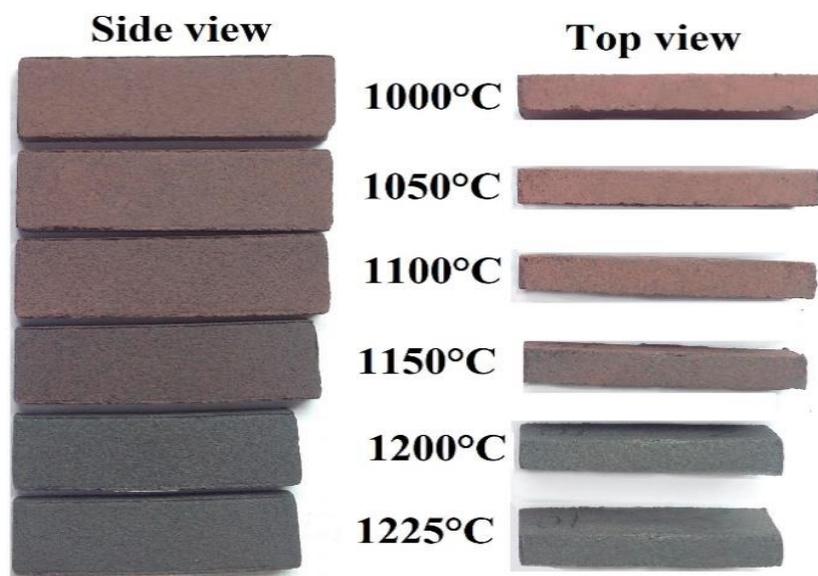
Physical-chemical processes of structure formation

Composition 7 was chosen to study the physical-chemical processes of the ceramics structure formation due to its high content of RM (50%) and its high flexural strength, exceeding class C demands (>4.0 MPa) of NBR 15270 [23].

Mineral composition changes during ceramics sintering: The XRD analyses of the ceramic composition sintered at 1,000 and 1,225ºC revealed the presence of magnetite (Fe_3O_4), hematite (Fe_2O_3), fayalite (Fe_2SiO_4), albite ($NaAlSi_3O_8$), and quartz SiO_2, with a high incidence of amorphous materials.

Most of the peaks overlapped to one another. The non-overlapping mineral peaks indicated the noticed reduction or increase in the number of minerals formed between 1,000º and 1,225ºC. It was noticed a significant decrease in the free

peaks of fayalite at 22 θ=34.2° and the almost complete hematite disappearance at 22 θ=24.2°. It is known that hematite turns into magnetite at high sintering temperatures in Table 7.

Table 7. Changes in position (d, Å) and intensities (I %) of XRD peaks ceramic 7.

Composition 7-1,000°C				Composition 7 -1,225°C		
2 θ	d, Å	I%	Symbol	d, Å	I%	Symbol
23.9	3.7	53.74	H; A	3.7	28.46	H; A
24.2	3.67	36.73	H	3.6	8.37	H
26.6	3.3	11.57	Q	-	-	-
33.2	2.69	100	H; A	2.69	100	H; A
34.2	2.62	15.53	F	2.62	5.17	F
35.7	2.51	68.89	M; H; F; A	2.51	56.76	M; H; F; A
40.9	2.2	21.34	F; A	2.2	17.64	F; A
42.2	2.14	3.84	A	2.16	8.86	A
49.6	1.837	28.13	H; F; A	1.838	23.33	H; F; A
54.2	1.692	33.51	H; F; A	1.691	28.12	H; F; A
57.6	1.598	6.61	H; F; A; Q	1.599	4.26	H; F; A
62.5	1.485	19.98	M; H; F; A	1.484	15.97	M; H; F; A
64.1	1.452	18.89	H; F; A; Q	1.452	13.68	H; F; A

This transformation was not visible due to the absence of free magnetite peaks and their coincidence with hematite, fayalite, quartz peaks, which suffered a decrease or even disappeared.

The decrease in minerals' crystalline peaks on XRD was almost undetectable. Quartz (2 θ°=26.6°) was the only mineral whose peak did not coincide with and other minerals, disappearing after sintering at 1,225°C (Table 7).

Albite was the only mineral, which undoubtedly had its intensity increased (22 θ°=42.2°) (Table 7). A reduction in the intensity scale from 1500 to near 1400 cps (counts per second) also indicated that some crystalline phases have turned into the amorphous state.

T0hermic reactions during ceramics 7 sintering: The presence of 10.0% SO_3 and high iron content 62.1%, Table 1 in the chemical composition of the blast furnace slag inevitably led to their combination during composition 7's heating in the forms of iron hydrates, iron sulfates, and iron sulphides.

The third exothermic effect of composition 7 occurred at 735°-1,227°C and involved four different thermochemical reactions: the transition γ -Al_2O_3→ α -Al_2O_3; the transition Fe_3O_4 → Fe up to 700°C-750°C [24]; reduction in sample weight as a result of the final SO_2 release and burning of the released gas; the formation of Fe_3O_4. The total weight loss of these processes was 4.43%. Probably, the formation of iron dross and the SO_2 combustion process imparted the darkening of the samples, which appeared at temperatures of 1,200°C–1,225°C [25,26]. The maximum intensity of these processes at 1,225°C resulted in maximum flexural strength of the ceramics 7.

Morphological structure modifications during ceramics sintering: SEM micro-images from composition 7 after sintering at 1,000ºC and 1,225ºC were analyzed, and it was clear the beginning of the initial mix melting process after 1000ºC, with many pores of different sizes between rounded different-sized particles. The escalation in the heating temperature (up to 1225ºC) led to a complete transformation of the earlier separated particles into a nearly pore-free glass-like monolithic structure. The only explanation for the morphological changes might be variations in the melting of all particles and the chemical interaction that took place.

Flexural strength enhanced almost 2.5 times 19.78 versus 8.12 MPa, Table 3 with significant improvement in other mechanical characteristics. The samples' edges of ceramics 7 were slightly melted, and the surface turned black Figures 2a-2c, apparently due to hematite-to-magnetite transition, which validated the XRD analysis' results.

Microchemical composition of the ceramics' new formations: The new formations were evaluated by the EDS method. Six different points was analysed, and all of them showed high heterogeneity Table 8, such as Na content ranging from 0.00 to 7.16%, and Ca content from 0.00 to 7.00%.

Table 8. The chemical composition of the points by EDS method.

Spectrum	Na	Al	Si	Ca	Fe	Zr	Total
1	0	0	19.6	0	10.79	69.62	100
2	7.16	9.04	13.23	5.48	65.09	0	100
3	1.96	2.26	4.91	0	4.67	86.2	100
4	0	6.75	11.48	7	74.78	0	100
5	0	0	0	0	59.35	40.65	100
6	0	2.76	23.56	0	16.61	57.07	100

Figure 2. Isotopes' composition of the ceramics' 7 new formations after sintering at 1,225ºC (laser micro-mass analysis method). **Note**: A=3 keV, B=6 keV, C=9 keV.
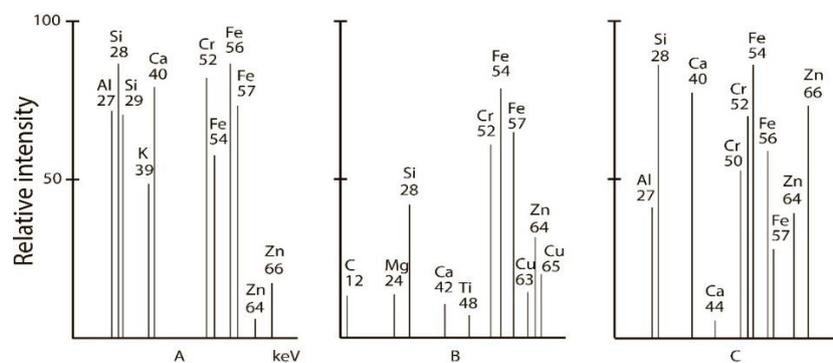
High heterogeneity, such as Na content ranging from 0.00 to 7.16% and Ca content from 0.00 to 7.00%, was identified in three distinct areas by the EDS method (Table 8). The use of LAMMA technique has provided similar results in isotopic compositions on the nearest points of the quoted ceramic.

Environmental characteristics of the developed ceramics: Heavy metals solubility and leaching of RM (Zn, Ba, Sn, and Cr) far exceeded the toxicity accepted by the Brazilian standard [20]. But very low melting points of these heavy metals (Zn-

419ºC, Sn-232º, Ba-727ºC) and other chemical elements (K-63º, Na-97º, Al-660º, Ca-842ºC) explains not only the intensification of all developed ceramics' structure formation processes, but also their high chemical stability in acid solutions.

Therefore, composition 7 was studied for understanding this phenomenon using the AAS method. Comparing these values before and after using RM on ceramics production revealed a stable chemical fixation of these metals in RM, culminating in more environment-friendly materials when compared with the requirements of the standard. According to leaching and solubility tests, the developed material presented no propensity to react with the environment. In this way, ceramics might be shredded and recycled as inert material in concrete production at the end of their useful life.

Gas control results during the developed ceramics production

Samples of the heat gases were collected during ceramics' sintering till 1,225ºC in the glass filter Figure 3 with a thickness of 0.45 µm. The separation of the solid particles deposited on the filter was performed by ultrasound (three hours in an acidic medium) and determined by the AAS method. These results, along with leaching and solubility tests, convincingly confirmed the robust bond of heavy metals in insoluble and non-volatile condition.

Figure 3. Electric oven with gas filter.
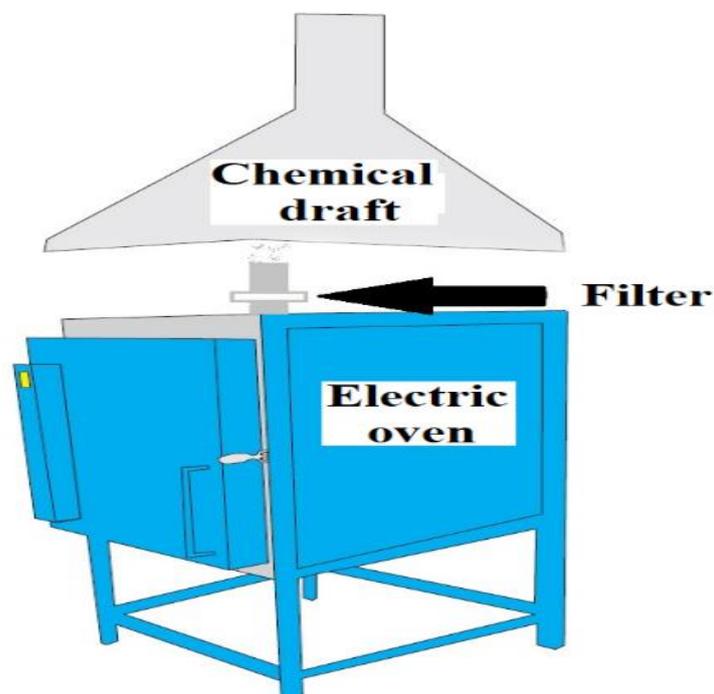
CONCLUSION

It has been experimentally demonstrated that bauxite tailings might be used as the main component (up to a content of 80 wt.%) in composites with blast furnace slag. This study aimed to replace the traditional raw materials (natural clay and sand) used to produce environment-friendly red ceramics with suitable mechanical properties. The fifty/fifty Red Mud and blast furnace slag composition showed 20 MPa in flexural tests, far exceeding the resistance of ceramics made from natural

raw materials due to intensification of all structure formation processes. Other useful parameters were observed, such as linear shrinkage values (11.40%), water absorption (1.95%), and moderate density (2.61g/cm^3). Physicochemical studies by XRD, SEM with EDC, and LAMMA microanalysis showed that the new ceramics had mainly vitreous structures with small crystal inclusions. The heavy metals leached from RM far exceeded the recommended levels of Brazilian sanitary standards. In the developed ceramics, all heavy metals were tightly bound in insoluble vitreous structures. Furthermore, solubility tests on the new ceramics showed their complete environmental compatibility. Analyses of heat gases collected during ceramics' sintering till 1,225ºC confirmed the robust bond of heavy metals in non-volatile condition. Therefore, the application of the suggested method on an industrial scale would have a positive impact on the ecosystems of industrial regions and cities; firstly, preventing the disposal of hazardous waste; secondly, extending the service life of industrial landfills. Finally, decreasing the irreparable impact of quarries of traditional raw materials (clay and sand) for traditional ceramics production. At the end of the life span of the new ceramics, they might be shredded and used as filler in concrete production, because they remain utterly inert, demonstrated by the leaching and solubility tests.

The developed materials production might be highly profitable because the use of ordinary industrial waste products would significantly reduce the production cost compared to the relatively expensive traditional natural materials.

ACKNOWLEDGEMENTS

REFERENCES

1. Hawking SW. Stephen Hawking says pollution and 'stupidity' still biggest threats to mankind. 2016.
2. World Aluminum. Primary aluminum production. 2018.
3. The Guardian. Hungary toxic sludge spill an 'ecological catastrophe' says government. Hungary. 2018.
4. Mariana. Brazil's mining tragedy: was it a preventable disaster? The Guardian. 2015.
5. Sushil S, et al. Catalytic applications of red mud, an aluminum industry waste: A review. J Appl Catalysis B: Environmental. 2008;8:11.
6. Liu W, et al. Review on treatment and utilization of bauxite residues in China. Int J Miner Proc. 2009;3:220-231.
7. Deihimi N, et al. Characterization studies of Red Mud modification processes as adsorbent for enhancing ferricyanide removal. J Envir Manag. 2018;206:266-275.
8. Barthoda J, et al. Adding worms during composting of organic waste with Red Mud and fly ash reduces CO_2 emissions and increases plant available nutrient contents. J Envir Manag. 2018;222:207-215.
9. Dodoo-Arhin D, et al. Fabrication and characterization of Ghanaian bauxite red mud-clay composite bricks for construction applications. Am J Mat Sci. 2013;3:110-119.
10. Liu Y, et al. Hidden values in bauxite residue (red mud): recovery of metals. J Waste Manag. 2014;34:2662-2673.
11. Rychkov V, et al. Intensification of carbonate scandium leaching from Red Mud (bauxite residue). J Hydrometallurgy. 2021;199:105524.
12. Pontikes Y, et al. Bauxite residue in cement and cementitious applications: current status and a possible way forward. J Res Conserv Recyc. 2013;73:53-63.
13. Heidrich C, et al. Iron and steel slags: global perspective on the circular economy. ISSUU. 2017.

14. Lukowski P, et al. Durability of mortars containing ground granulated blast-furnace slag in acid and sulphate environment. J Procedia Eng. 2015;108:47-54.

15. Barreto LSS, et al. Reuse of ornamental rock-solid waste for stabilization and solidification of galvanic solid waste: Optimization for sustainable waste management strategy. J Clean Prod. 2020;275:122996.

16. El-Ashtoukhy ESZ, et al. Intensification of a new electrocoagulation system characterized by minimum energy consumption and maximum removal efficiency of heavy metals from simulated wastewater. J Chem Eng Proc–Proc Inten. 2020;154:108026.

17. Kołodyńska D, et al. Evaluation of possible use of the macroporous ion exchanger in the adsorption process of rare earth elements and heavy metal ions from spent batteries solutions. J Chem Eng Proc & Proc Inten. 2020.

18. Koizumi S, et al. Design of a novel fertilizer made of steelmaking slag using the glassy phase of the $CaO-SiO_2-FeO$ system. J Sustain Metall. 2021;7:87-98.

19. Ding L. Preparation and characterization of glass-ceramic foams from blast furnace slag and waste glass. J Mat Let. 2015;141:327-329.

20. The solid waste classification according to ABNT NBR 10004/2004. MyWaste. 2004.

21. Johnson DW, et al. Kinetics of the decomposition of freeze-dried aluminum sulfate and ammonium aluminum sulfate. J Amer Ceram Soc. 1971;54:461-465.

22. Kato E, et al. Decomposition of two aluminum sulfates and characterization of the resultant aluminas. J Amer Ceram Soc. 1981;64:436-443.

23. NBR 15270 Ceramic components, Part 2: Ceramic blocks for structural masonry and sealing-Terminology and requirements. 2005.

24. Brown ME, et al. Handbook of thermal analysis and calorimetry: recent advances, techniques and applications. Elsevier. 2011.

25. Lykasov AA, et al. Phase equilibria in systems Fe-Al-O and Fe-Si-O in the temperature range 1100 K-1300 K. 2003;39:1088-1091.

26. Chanturia EL, et al. Features of sulfide ferruginous quartzite mineralization. J Mining Sci. 2009;45:495-498.